



## Research Article

## Applying geometric morphometrics to compare changes in size and shape arising from finite elements analyses

Paul O'HIGGINS<sup>a,\*</sup>, Nicholas MILNE<sup>b</sup>

<sup>a</sup>Centre for Anatomical and Human Sciences, Hull York Medical School, University of York, York, England, YO10 5DD, UK

<sup>b</sup>School of Anatomy Physiology and Human Biology, University of Western Australia, Crawley 6009, Australia

### Keywords:

geometric morphometrics  
finite elements analysis  
armadillo femur

### Article history:

Received: 30 May 2012

Accepted: 4 September 2012

### Acknowledgements

We are grateful to Sergio Vizcaino and Michael Fagan who made useful suggestions in early discussions related to this work, Laura Fitton and Flora Gröning provided advice and support in our model reconstruction and FEAs. Fred Bookstein has also provided ongoing, critical and insightful feedback on our efforts to apply GM in functional studies. Any errors that remain are the authors' own responsibility. Vox-FE was developed by Michael Fagan, Roger Phillips and Paul O'Higgins with support from BBSRC (BB/E013805; BB/E009204). Nick Milne was supported by a study leave grant from The University of Western Australia.

### Abstract

We consider how the methods of geometric morphometrics (GM) might combine with functional simulations using finite elements analysis (FEA). In particular we are concerned with how the deformations arising from FEA might be compared and visualized using GM. To these ends we apply these methods to a study of coronal plane forces applied to a model of an armadillo femur. We simulate the stance phase in the hind limb where the femur is subject to bending strains due to longitudinal compressive as well as abduction loads on the greater trochanter. We use this model to examine the hypothesis that muscles attaching to the third trochanter can reduce these bending strains in the loaded femur. The analysis uses standard finite element methods to produce strain maps and examine the strains at 200 point locations on the femur, but we also use the locations of the 200 points to run novel geometric morphometric analyses to assess the gross deformation of the model under different loadings. These provide insights into the application and usefulness of geometric morphometric methods in interpreting the results of finite element analyses. With further mathematical, engineering and statistical development the combination of FEA and GMM should open up new avenues of investigation of skeletal form and function in evolutionary biology.

## Introduction

In this paper we consider how studies of skeletal performance using finite elements analysis (FEA) might be compared using geometric morphometric (GM) approaches. After considering what GM can and cannot do in this context, we illustrate and explore the joint use of these approaches through an example study of femoral form and function in an armadillo. GM methods alone can be used to relate variations in skeletal form to aspects of function by assessing how the form of a configuration of landmarks taken on the skeletal part covaries with functionally interesting variables. Thus, in a study of long bones, how skeletal form covaries with e.g. body mass, or limb length, or running speed etc. can be understood and compared through e.g. regression of form on relevant variables. However, this approach does not directly relate skeletal form to performance under loading. For this, simulated functional loading using finite elements analysis (FEA) with subsequent measurement and comparison of skeletal performance is required. One interesting aspect of performance is how an object deforms when loaded.

In continuum mechanics the term “deformation” means both rigid body motion (translation and rotation) together with changes in form (size and shape). Here, however we use the common definition of “deformation”, which refers to changes in size and shape of an object but not rigid body motions. This is a more familiar usage for workers in GM. In engineering how the size and shape of a loaded elastic body responds to loads is commonly measured using strains (e.g. principal strains, Von Mises strains). These are used to predict failure and often in biology to assess and compare performance of either the same model under different loadings or, different models under similar loadings (e.g. in studies of the skeletal response to loads, Gupta et al. 1973;

Hart et al. 1992; Koriath and Hannam 1994; Vollmer et al. 2000; Koolstra and van Eijden 2005; Moazen et al. 2009; Rayfield 2005; Ichim et al. 2007; Strait et al. 2007, 2009; Kupczik et al. 2007; Wroe et al. 2007). Strains sampled at several points may be compared singly or submitted to multivariate analysis (e.g. Gröning et al. 2012; Parr et al. 2012). However this leads to an incomplete analysis, and no proper statistical framework yet exists to compare strain fields (Bookstein, 2011; Weber et al., 2011) or to account for the effects of uncertainties in modelling on computed strains. Strains and strain maps are also frequently used as a visual guide to large scale deformations such as long bone bending or cranial “twisting” that arises from loading. Strain magnitudes and directions describe deformations at each point but are not well suited to assessment of large scale patterns of deformation (see O'Higgins et al. 2011 for more detail). An alternative is to assess large scale deformations by describing the changes in the form of a landmark configuration on a body before and after loading. This shares much in common with the application of GM approaches to kinematic analyses of motion using temporal sequences of landmark configurations, representing e.g. changing limb postures. At each temporal sampling point, the form of the configuration is recorded and the full set of configurations sampled over the period of interest is submitted to GM analysis. The analysis then focuses on comparing trajectories of form change over time. Slice (1999) and Adams and Cerney (2007) have shown how this approach can facilitate quantification and analysis of complex motions involving many joints or complex motion at few joints (e.g. the jaw in chewing). It is equally applicable to kinematic analyses of deformable surfaces or volumes such as the face during expression or speech (O'Higgins et al., 2002), or to a body deforming under loads such as is simulated in FEA. There are subtleties to such an analysis that concern: registration (i.e., if and how we scale, translate and rotate), its meaning and effects, and how motions are broken down into sequential landmark configurations (Slice, 2003).

\* Corresponding author

Email address: paul.ohiggins@hymms.ac.uk (Paul O'HIGGINS)

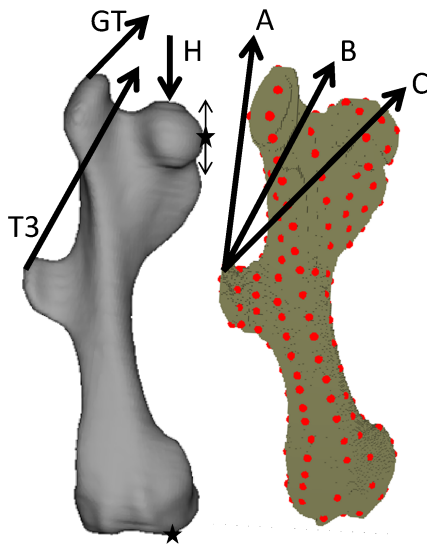


**Figure 1** – The armadillo femur models showing the constraints (stars), forces applied (arrows) to the head (H), greater trochanter (GT), and third trochanter (T3). Also shown is the finite element model with; the 200 landmarks placed on the surface, and the three possible directions for the third trochanter load.

While it is unlikely that large scale deformations of skeletal parts drive either evolutionary or ontogenetic adaptations, differences can be informative from the perspective of analyses of anatomical-functional correlations (e.g. Milne and O’Higgins 2012). Further, GM analyses of how a skeletal structure deforms can provide a useful adjunct to sensitivity and validation studies where subtle differences are not readily appreciated from strains sampled at a few locations or from strain maps (Gröning et al., 2011; Fitton et al., 2012). It should be noted that GM approaches to the comparison of deformations do not have the same aim as strain based comparisons; they are not directed at predicting failure. Neither can transformation grids describe the actual deformation of tissue between landmarks. This is because the method of interpolation does not reflect the actual stretching or compression of the physical material. Of course, this same issue applies to GM studies of skeletal ontogeny and evolution where grids serve as a device for visualisation of changes in size and shape of landmark configurations rather than as a representation of the biological processes underlying bone growth or evolutionary transformation; it facilitates visualisation of pattern, not process, by interpolating the changes in form of a landmark configuration to the space between and in the vicinity of the landmarks. Additionally, the landmarks themselves, unless they comprise all of the nodes of all of the finite elements, incompletely describe the deformation (O’Higgins et al., 2011). It should be borne in mind that, as with studies of e.g. growth or evolution, different landmark configurations will give rise to different distances between forms and so adequate design of the landmark configuration is important (Oxnard and O’Higgins, 2009).

We demonstrate the application of GM to the results of FEA in a study of the femur of an armadillo (*ChaetophRACTUS villosus*). The femur presents a large third trochanter (T3; Fig 1), a common feature of xenarthrans, that varies in position along the shaft being more distal in larger animals. Many studies have highlighted how human femoral bending occurs in response to longitudinal compressive loads acting through the femoral head and abductor loads acting on the greater trochanter, and how loads simulating tension in the iliotibial tract have an “unbending” effect (using polarised light methods and beam theory, Pauwels 1980; Rybicki et al. 1972; finite element methods, Taylor et al. 1996; free body analysis, Duda et al. 1997). Similarly, Milne et al. (2011) suggested that muscles attached to T3 in xenarthrans act to reduce coronal plane bending stress in the armadillo femur. Recently this suggestion has been supported by a study (Milne and O’Higgins, 2012)

that compared the “unbending” effect of muscles attached to T3 in large and small xenarthrans. The background to this work is presented here to illustrate how GM approaches can be usefully applied to interpretation of changes in skeletal form arising from simulated loading in FEA.

We carry out FEA to assess the function of the third trochanter and the impact of variations in loading and segmentation of internal architecture. We also compare the performance of a solid model with that of a model with more detailed internal structure because it is not straightforward to delineate cortical from trabecular bone in CT scans, especially in fossils which we intend to include in subsequent work. Using GM approaches, we show the effects of varying the magnitudes of simple and combined loads on the resulting strain maps and on large scale deformations of solid and hollow femoral models. These analyses allow us to assess the extent to which gluteus maximus and tensor fasciae latae muscles attached to the third trochanter reduce bending.

## Methods

**Model building, sensitivity to modelling decisions and loading simulation.** One femur from a hairy armadillo (*ChaetophRACTUS villosus*) was CT scanned (1 mm slices with a resolution of 0.1145 mm). The CT stack was segmented (i.e. the grey levels representing bone were used to isolate bone material in each CT slice in preparation for building a 3-D model of the bone) in AMIRA 4.1.1 (Mercury Computer Systems Inc., USA). The resolution of the scan meant that the cancellous bone in the epiphyses could not be segmented in any detail. In consequence the initial model was mostly solid at the epiphyses but retained the empty medullary space in the shaft. Extraneous material, including remnants of the cruciate ligaments, was removed. Following sensitivity studies that showed little difference in resulting strains or large scale deformation with voxel side length varying between 0.2 and 0.8 mm, the Amira mesh was resampled to make a model with cubic voxels of side 0.4 mm. This model was then re-segmented to fill the hollow in the shaft with solid material. The 3D volume data for the two models were exported as bitmap stacks and then converted to 8-noded linear brick finite element meshes by direct voxel conversion. The resulting models had 83627 (hollow) and 86914 (solid) elements. It has been shown in previous work that our voxel based approach achieves almost identical results to those obtained using other element types (Liu et al., 2011).

The finite element analyses (FEA) were performed using the non-commercial FEA software VOX-FE (Fagan et al. 2007; numerically validated in Liu et al. 2011; release will be announced on <http://www2.hull.ac.uk/science/cmet.aspx>). The models were assigned isotropic material properties within the range of published values for bone (17 GPa for Young’s modulus and a Poisson’s ratio of 0.3) although material properties vary from location to location (are heterogeneous, e.g. Dechow et al. 1993). This is justified on the grounds that Panagiotopoulou et al. (2012) have shown that in an elephant femur, although strains predicted by an homogeneous model less well matched experimental data than those from an heterogeneous model, the mismatch was principally in the mean magnitude of predicted strains and, to lesser degree, in the pattern of deformation (relative strain values). Thus, to predict the overall pattern, but not magnitude of deformation, the heterogeneity typical of long bones appears less important.

To approximate physiological conditions, the models were constrained in the x, y, and z directions at an area of the distal surface of the medial femoral condyle, and also in the x and y directions on the medial surface of the femoral head, thus enabling the head to move up or down under load. These constraints were chosen because, in Xenarthra the medial condyle bears most of the load at the knee (Koneval 2003; Milne et al. 2011 and references therein), and the sliding constraint on the femoral head represents the pelvis, which prevents the femoral head from being displaced medially. Simple loads (Fig. 1) were used to assess model performance, thus a compressive force representing body mass and the net action of thigh musculature was applied to the upper surface of the femoral head, and that force was directed through the centre of the constrained area of the medial femoral condyle. A force representing the lesser gluteal (abductor) muscles was applied to the superolateral part of the greater trochanter and that force was directed

superomedially, in the coronal plane at an angle of 45 degrees above the horizontal (Fig. 1). The size of the head and greater trochanter loads was 60 and 120 newtons, equivalent to the effects of approximately twice and 4 times the body weight of the armadillo. The number of constrained or loaded nodes was chosen to mirror normal anatomy while keeping the number of such nodes small, about 60 for each constraint and load. The models were iteratively solved to equilibrium on a PC.

Two hundred landmarks were placed on the surfaces of the models using Amira (Fig. 1). The landmarks were chosen to provide even and fairly dense coverage of the whole bone. There is no issue of equivalence of landmarks between load cases as the landmarks are tied to the bone mesh and move with it as it deforms. Further in a recent paper comparing the function of armadillo femora (Milne and O'Higgins, 2012) we have shown that the results of size and shape analyses using 40 "homologous" landmarks to compare femoral performance are very similar to those from the 200 landmarks used to assess deformation of single femora. This finding is consistent with a sensitivity analysis (in Fitton et al. 2012) that found, in reducing from 300 to 70 landmarks, little effect on performance analyses relating to cranial loading. This is reassuring in the context of the present study but it should be borne in mind that similar considerations apply to landmark choice in analyses of performance as apply in relation to analyses of form (Oxnard and O'Higgins, 2009) and additional internal landmarks might bring additional information into the analyses. After each load case was run, the principal strains at, and the new coordinates of, each landmark were extracted. For each model 5 load cases were run: 60 or 120 newtons at the head or greater trochanter and 60 newtons at both the head and greater trochanter (GT). Subsequently, additional loads were applied to T3. Since muscle force vectors are estimated from dissections (Koneval, 2003) and observations of articulated skeletons, three different force directions were applied to the third trochanter to assess the sensitivity of the model to force direction (Fig. 1).

Maps of either Von Mises or surface principal strains were also produced. Von Mises strains reflect the magnitude of deformation at each point and require just one diagram to map them. They simplify the presentation of results but information about the nature of strains, whether they are tensile or compressive, requires maps of the relevant principal strains. Surface Von Mises strains were mapped from the analysis of load doubling and for the comparison of hollow and solid models, because they succinctly summarise the patterns of strain density. Surface principal strains were mapped from the analysis of multiple loads because the diagrams show whether the strain at each point is tensile or compressive and so facilitate interpretation of large scale deformation of the model.

**Geometric morphometric analysis of deformations.** The 3D coordinates of the 200 landmarks in the unloaded model and each load-case were submitted to geometric morphometric (GM) analysis to assess global deformations. The most common approach to GM analysis focuses on shape; it scales landmark configurations to unit centroid size; the square root of the sum of squared landmark distances from their centroid. Next, shape variables are computed by translating and rotating (registering) all configurations to minimise the sum of squared landmark distances with respect to the mean (Dryden and Mardia, 1998). Differences in shape are expressed by Procrustes distances, computed as the square root of the sum of squared differences in shape variables between configuration pairs. Differences in size are expressed by differences in centroid size, the square root of the sum of deviations of the landmarks from the centroid.

However, in this application to the comparison of results of FEA, an approach that simultaneously accounts for differences in both size and shape is required. This is because, under loading the body deforms and landmarks displace. Differences in both size and shape are consequent on the applied loads; in terms of mechanics it makes little sense to partition form changes into these components or to weight them differently. Therefore, in previous applications of GM methods (O'Higgins et al., 2011; Gröning et al., 2011; Fitton et al., 2012) principal components analysis of the shape variables plus the log of centroid size (Procrustes

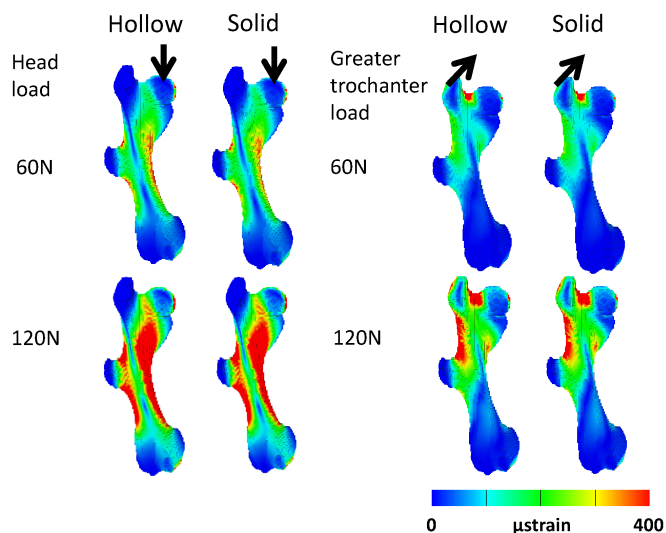


**Figure 2** – Simple loadings on the head or greater in hollow and solid models. Strain maps showing the effects of head or greater trochanter loads of 60 and 120 newtons. The pairs of images allow comparison of the strain patterns in hollow and solid models. Von Mises strain 0 to 0.4 microstrains.

form analysis) was employed to assess how loadings impact on both model size and shape. However, logging of centroid size rescales this component relative to shape in such a way that size differences resulting from loading are given a relatively lower weight than would be the case if the initial scaling had not been carried out.

An alternative that preserves the weighting of both is to omit the scaling step prior to registration and carry out analyses using the resulting "size and shape" variables (Dryden and Mardia 1998; Dryden et al. 2007). Note the resulting variables combine size and shape information and in contrast to Procrustes Form analysis do not comprise shape variables plus a size variable). While omission of the scaling step does not lead to specimens being represented in the well-behaved Kendall's shape space that results from Procrustes superimposition, the fact that the deformations resulting from FEA are very small mitigates the impact of variations in size on such things as the estimation of means and covariances. Further, a consequence of omitting the scaling step is that resulting distances between loaded and unloaded forms might reflect pure shape or pure size, or some mix of size and shape depending on the directions of the vectors connecting the models in the resulting size and shape space. While this may be undesirable in some applications it is consistent with the idea that loadings can produce changes in size and/or shape. Thus, conceivably, but impractically, loads could be applied everywhere within and over an object to make it isometrically smaller or larger, but more often loads have some effect on size and some on shape. In order therefore to assess the effects of loads, size and shape changes need to be considered together.

Here, we use this approach because it is better justified from considerations of the mechanics, but the consequences on the eventual results are imperceptible with regard to relative distances among load cases and visualisations of aspects of deformation captured by PCs when compared to the results of Procrustes form (shape plus log centroid size) or shape analyses. This lack of difference between approaches is attributable to the very small differences in size relative to shape that arise from our FEAs. Thus, we carry out a "size and shape" analysis by translating and rotating but not scaling landmark configurations to minimise the sum of squared distances among landmarks. This rigid body fitting of landmark configurations from unloaded and loaded forms (see O'Higgins et al. 2012) produces "size and shape" variables. Size and shape distances among unloaded and loaded models are computed and PCA of size and shape variables is carried out to complement the strain based analyses. The aspects of size and shape variation described by each PC can be visualised, facilitating interpretation of PC plots in terms of deformations of the models. We visualise these deformations as warped rendered surface models together with a trans-

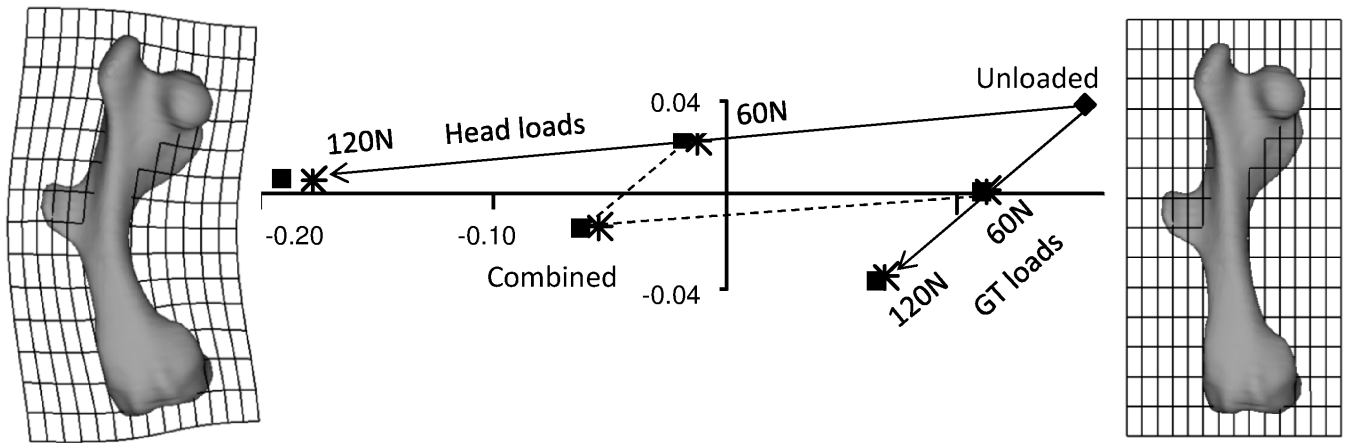


**Figure 3** – GM analysis of simple and combined loads. PC1 (95.9%) and PC2 (4.1%) from a size and shape space analysis of the coordinates of the 200 landmarks. The shapes to the left and right show the shape change in the model associated with PC1, from the unloaded state on the right to the loaded state with the deformed grid on the left. These deformations are exaggerated by a factor approximately 100 to aid visualisation. Diamond = unloaded, square = hollow, star = solid models. Note that two PCs are sufficient to describe the aspects of large scale deformation in this analysis because only two forces are applied, This results in two modes of deformation, albeit with varying relative magnitude among load cases, which are described by two PCs.

formation grid computed using a triplet of thin plate splines (one for displacements in each of x, y and z; Dryden and Mardia 1998). As noted earlier, the deformation of the grid is interpolated from the deformation of the landmark configuration and so only approximates the actual deformation of the model between the landmarks; in this sense it is quite unsuited to studying the elastic behaviour of the bone material. Rather, the grid is a device to facilitate visual interpretation of the large scale aspects of deformation of the landmark configuration.

Specific analyses using both strains and GM methods assessed: 1. Differences between the deformations of the solid and hollow models. 2. The effects of doubling of loads. 3. The effects of combining loads. 4. The impact of muscles acting on the third trochanter on “un-bending” of the femoral shaft.

## Results

### Differences between the deformations of the solid and hollow models

Strain maps for the two magnitudes of head and greater trochanter (GT) loads (Fig. 2) show very similar results for the hollow and solid models. They are hard to distinguish by eye. Quantitatively, the magnitudes of tensile and compressive strains at the 200 sampled nodes are slightly lower on average for the solid than the hollow model. The ratios of the mean strains at these 200 point locations in solid compared to the hollow models are all slightly less than one (60 N loads, tensile: head 0.992, GT 0.955; compressive: head 0.959, GT 0.970; for 120 N loads these proportions are exactly the same as for the 60 N loads). Further, the strain ratios between models at each sampled node closely approximate the ratios of mean strains (e.g. 60 N loads, mean solid/hollow strain ratio: tensile: head 0.990, GT 0.948; compressive: head 0.984, GT 0.962). These findings support the similarities seen in the strain maps (Fig. 2) and indicate that the principal difference between hollow and solid models is that the solid is a little stiffer but deforms like the hollow; a finding that echoes a similar result in lizard crania (Parr et al., 2012).

When the 200 landmark co-ordinates for the unloaded and the five load conditions are submitted to geometric morphometric analysis the resulting plot of PCs 1 and 2 (accounting for 95.9% and 4.1% of the shape variation respectively) shows that: the solid models are slightly stiffer than the hollow in that they are less distant from the unloaded model (Fig. 3). Size and shape distances indicate that the solid model deforms less than the hollow (ratio solid/hollow 0.965 under the same head load, and 0.964 for the GT load).

### The effects of doubling of loads

As expected, the strains at the 200 landmarks resulting from the 120 newtons loads are almost exactly twice the value of those that result from 60 newtons loads (all within 0.18%). Likewise, when the size and shape distances are compared between models with identical constraints and load vectors, these double as load magnitudes are doubled. Thus for the hollow model with head load alone the size and shape distance between the unloaded and 60 N (0.1729894666) models is half of that between the unloaded and 120 N loaded model (0.3459819139; ratio is 2.00001723). The same applies to centroid size (cs) with the change between the unloaded and the 60 N loaded models being very close to half that of the 120 N (hollow model ratios of 120 N to 60 N loadcases: head load = 1.998; GT 2.002). From Fig. 3, it is also apparent that doubling either load results in doubling of the lengths of the vectors between the unloaded and loaded models.

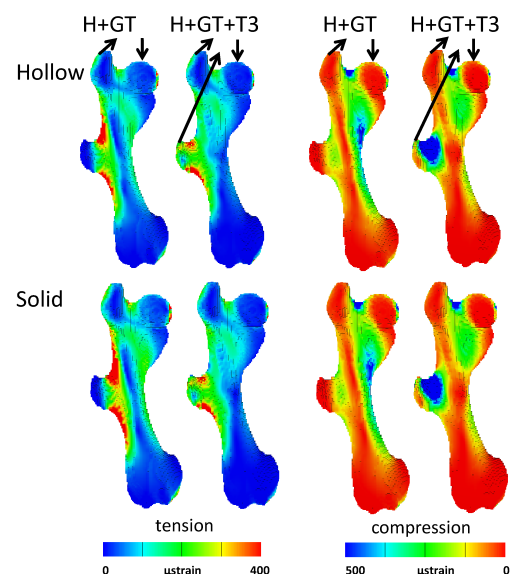


**Figure 4** – The effect of third trochanter loads. Strain maps of the armadillo femur under combined head and greater trochanter (H+GT) loads, and with an additional load on the third trochanter (H+GT+T3). All the loads applied are 60 N. Both compressive (-0.5 to 0 microstrains) and tensile (0 to 0.4 microstrains) strains are shown for the hollow and solid models.

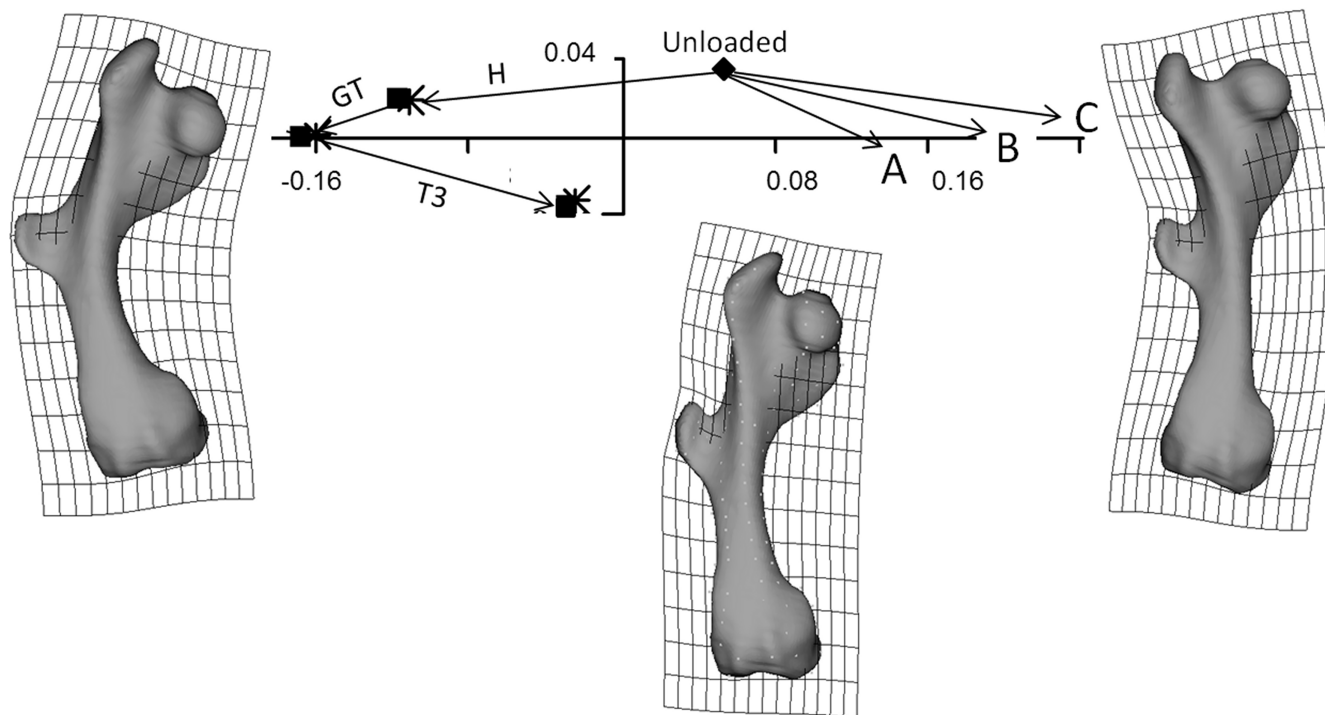


**Figure 5** – The addition of third trochanter loads. PCs 1 & 2 (97.1% & 2.3%) from a GM analysis of hollow (squares) and solid (stars) models. First a head load is applied (Vector H), then a greater trochanter load is added (GT), and then the third trochanter load is added (B, labelled as T3). The points A, B and C represent the deformations due to the three different force directions applied to the third trochanter of the unloaded model (diamond). The deformed models with grids indicate the changes in size and shape represented by PC1 (left and right), and PC2 (below the plot). These deformations are exaggerated by a factor of approximately 100 to aid visualisation.

### The effects of combining loads

The deformation caused by the combined load of 60 newtons on both the head and the greater trochanter is the same as the vector sum of the deformations caused by the two loads independently. This is illustrated by the parallelogram evident in Fig. 3. It is made up of the solid lines connecting the unloaded model and each of the 60 N load-cases and the dotted line connecting each of these and the combined load model. The ratios of the lengths of the short and long sides are respectively; (GT load) 0.999964, 0.999978 for the hollow model and 1.000013, 0.999993 for the solid model.

### The impact of muscles acting on the third trochanter on “un-bending” of the femoral shaft

From Fig. 2 and 3, it is evident that both head and greater trochanter loads result in medial bending of the femur. From a comparison of Fig. 2 and 3 it is clear that head and greater trochanter loads combine to produce more large scale bending than either force alone. When additional forces are applied to T3 the bending strains in the femoral shaft are reduced. Fig. 4 shows the compressive and tensile strains in models with head and greater trochanter loads compared with models with additional third trochanter loads. The addition of T3 loads results in reductions in tensile strains on the lateral side, and compressive strains on the medial side of the model. The plot of PCs 1 and 2 of an analysis of all three loadcases (Fig. 5) shows that while the head and GT loads cause increased bending in the model, the T3 loads reduce that bending (Fig. 5). Fig. 5 also shows that the three different force directions for the T3 load (A, B and C) all reduce bending in the femoral models. The transformation grids in Fig. 5 show that the aspects of deformation represented by PC1 predominantly consist of large scale bending of the femoral shaft, while those represented by PC2 are principally deformations localised to the greater and third trochanters, with no apparent bending of the femoral shaft.

### Discussion

We have simulated femoral loading, assessing the impact of loads, singly and then in combination, on deformation. The key underpinning technologies included imaging, image reconstruction and finite elements analysis which are commonly employed in functional analyses of skeletal elements (e.g. Hart et al. 1992; Kupczik et al. 2007; Wroe et al. 2007; Strait et al. 2009). Additionally we have applied some methods from geometric morphometrics to consider and compare large scale deformations (O’Higgins et al., 2011).

This study provides the opportunity to show how geometric morphometric methods relate to the more conventional engineering approach for quantitatively describing and comparing deformations; how they perform and inform. The situation whereby doubling of loads results in doubling of deformation is well known for principal strains (Fig. 2) and this linear relationship between load and deformation is also apparent using GM approaches (size shape distances from the unloaded model). Like strains, the empirically derived ratios of distances arising from doubling of loads are not exactly 2 but are very close, the error being most likely attributable to computational imprecisions in FEA and subsequent GM analyses. This similarity between the scaling of size and shape distances and strains and is of course to be expected, since both methods assess changes in size and shape, albeit at very different scales. It is worth noting that size and shape distances and strains also scale linearly with Young’s elastic modulus ( $\epsilon$ ; a measure of model stiffness) and length. Thus halving  $\epsilon$  doubles the size and shape distance between unloaded and loaded forms as does halving length (e.g. by isometrically scaling the form according to centroid size). These scaling relationships have a practical application in that a single load case can be used to visualise the range of deformations or estimate new deformations when constraints and load application points are kept constant but load magnitude,  $\epsilon$  or length (“size”) are varied. This avoids the need to run multiple alternative FEAs.

Since doubling of loads is effectively the combination of a load with itself, when two or more different loads are applied to the model, the resulting deformation is represented in the size and shape space as the vector sum of the deformations caused by those loads applied individu-

ally. Thus, in Fig. 3, the deformations caused by the individual loads form the sides of a parallelogram and the deformation of the combined load is represented by the diagonal of the parallelogram. This demonstrates that, as with strains, (and as expected with) size and shape distances, large scale deformations due to multiple loads can be estimated by combining the simpler constituent ones. Bear in mind that in our analysis few load cases are compared. As such the plane of PC1 vs PC2 in Fig. 3 is a perfectly adequate space in which to view results and combine deformations. As more complex analyses are undertaken, combining many load cases, it is likely that more dimensions of the size and shape space will be needed to represent the range of deformations they produce, and, as such, vector additions to combine loads will need to take account of the full dimensionality, by using all PCs.

Our analyses provide some insights into modelling and the function of the third trochanter in the armadillo. In particular it was not possible to work with the full 3D geometry of the femur because imaging resolution was inadequate to accurately segment cancellous bone detail, although the medullary cavity could be reconstructed. This situation is likely to be much worse in fossils where matrix will limit image segmentation with the result that solid models will be required. We therefore assessed the impact of working with a solid model rather than one with a hollow representing the medullary cavity. The results are encouraging in that the solid model behaves very like the hollow; the overall pattern of strains is very similar (Fig. 2 and 4). In the GM analyses (Fig. 3 and 5), the solid model deforms along the same trajectory but is a little stiffer than the hollow model. This is likely because the deformations that have arisen from our loading scenarios consist in the main of pure bending of the shaft. Because bending resistance depends on the second moment of area, which in the case of cylinders depends on the square of the distance of material from the neutral axis (see Lieberman et al. 2004 for a straightforward account), adding more material inside the bone does not have a significant impact on bending resistance. The situation would likely be different for pure compressive loads, where cross sectional area is relevant. With regard to the impact of muscles acting on the third trochanter on “unbending” of the femoral shaft, the results show that the head force produces bending in the femoral shaft, and that the action of abductor muscles acting on the greater trochanter increases this bending (Fig. 2, 3 and 4). We have demonstrated that muscles pulling on the third trochanter can counter this bending (Fig. 4 and 5). Fig. 5 also demonstrates that third trochanter loads (A-C) alone bend the femoral model in the opposite direction to head and greater trochanter loads, and that this still occurs to varying degree over the full range of possible T3 muscle force directions.

Using GM methods to analyse deformations of landmark configurations arising from FEA, provides an account of deformation that is complementary, but by no means substitutes for strain based analyses. It leads to understanding and visualisation of larger scale aspects of deformation, but does not inform in relation to likely sites of failure of the bony tissue.

We have only considered how size and shape analyses might be applied to different loadings of the same bone but a common situation involves comparison of the effects of applying the “same” loadings to different bones. We have recently published such a comparison between the armadillo (body mass 3 kg) femur described in this study and the femur of its giant extinct relative the 300 kg glyptodont (Milne and O’Higgins, 2012). Our approach was to use forces that produced similar strains and large scale degrees of bending in each and then to combine the coordinate data in a single size and shape analysis in order to compare large scale bending and “unbending”. This was done by first scaling translating and rotating (GPA) equivalent landmark configurations from each bone to register the load cases for each model. The differences between the coordinates of the landmarks in each loaded state and the unloaded model, were then added to the mean unloaded model shape for visualisation and the results were rescaled according to the ratio of centroid sizes between loaded and unloaded to “restore” size changes due to loading. The resulting coordinates were then submitted to a size and shape PCA of both femora. The finding was that in both animals a similar unbending effect is observed but this is greater

when the third trochanter is more distal. Such analyses open up the possibility of comparing the effects of loading among different specimens and of investigating covariations between loading response and other variables (e.g. skeletal form, ecology, phylogeny, etc).

There is a need for proper mathematical, engineering and statistical development of the approaches outlined in this paper but with this, and combined with the use of warping approaches to model building (O’Higgins et al., 2011, 2012; Parr et al., 2012; Pierce et al., 2008; Sigal et al., 2008; Sigal et al., 2010; Stayton, 2009), combinations of FEA, GM and modern imaging techniques should eventually lead to new analyses that experiment with and take account of variations in form and loading and so provide novel insights into how skeletal form relates to function, ecology and evolution. ☺

## References

- Adams D.C., Cerney M.M., 2007. Quantifying biomechanical motion using Procrustes motion analysis. *Journal of Biomechanics* 40: 437–444.
- Bookstein F.L., 2011. Speculations on the next statistical toolkit for complex organized systems. *Proceedings of the 29<sup>th</sup> Leeds Annual Statistical Research Workshop*. <http://www.maths.leeds.ac.uk/statistics/workshop/lasr2011/Proceedings/Bookstein.pdf>
- Dechow P.C., Nail G.A., Schwartz-Dabney C.L., Ashman R.B., 1993. Elastic properties of human supraorbital and mandibular bone. *American Journal of Physical Anthropology* 90(3): 291–306.
- Dryden I.L., Mardia K.V., 1998. *Statistical shape analysis*. John Wiley, London.
- Dryden I.L., Hirst J.D., Melville J.L., 2007. Statistical analysis of unlabeled point sets: comparing molecules in chemoinformatics. *Biometrics* 63: 237–251.
- Duda G.N., Schneider E., Chao E.Y.S., 1997. Internal forces and moment in the femur during walking. *Journal of Biomechanics* 30: 933–941.
- Fagan M.J., Curtis N., Dobson C.A., Karunanayake J.H., Kupczik K., Moazen M., Page L., Phillips R., O’Higgins P., 2007. Voxel-based Finite Analysis – Working Directly with MicroCT Scan Data. *Journal of Morphology* 268: 1071.
- Fitton L.C., Shi J.F., Fagan M.J., O’Higgins P., 2012. Masticatory loadings and cranial deformation in *Macaca fascicularis*: a finite element analysis sensitivity study. *Journal of Anatomy* 221: 55–68.
- Gröning F., Fagan M.J., O’Higgins P., 2011. The effects of the periodontal ligament on mandibular stiffness: a study combining finite element analysis and geometric morphometrics. *Journal of Biomechanics* 44: 1304–1312.
- Gröning F., Fagan M., O’Higgins P., 2012. Modeling the Human Mandible Under Masticatory Loads: Which Input Variables are Important? *The Anatomical Record* 295(5): 853–863. doi:10.1002/ar.22455
- Gupta K.K., Knoell A.C., Grenoble D.E., 1973. Mathematical modeling and structural analysis of the mandible. *Biomaterials, Medical Devices and Artificial Organs* 1: 469–479.
- Hart R.T., Hennebel V.V., Thongpreda N., van Buskirk W., Anderson R.C., 1992. Modeling the biomechanics of the mandible: a three-dimensional finite element study. *Journal of Biomechanics* 25: 261–286.
- Ichim I., Kieser J.A., Swain M.V., 2007. Functional significance of strain distribution in the human mandible under masticatory load: Numerical predictions. *Archives of Oral Biology* 52: 465–473.
- Koneval T.O., 2003. Comparative hindlimb anatomy and fossoriality of three armadillos: *Dasyops novemcinctus*, *Tolypeutes matacus*, and *ChaetophRACTUS vellerosus* (Mammalia, Xenarthra Cingulata, Dasypodidae). PhD thesis, University of Massachusetts.
- Koolstra J.M., van Eijden T.M.G.J., 2005. Combined finite-element and rigid-body analysis of human jaw joint dynamics. *Journal of Biomechanics* 38: 2431–2439.
- Korioth T.W., Hannam A.G., 1994. Deformation of the human mandible during simulated tooth clenching. *Journal of Dental Research* 73: 56–66.
- Kupczik K., Dobson C.A., Fagan M.J., Crompton R.H., Oxnard C.E., O’Higgins P., 2007. Assessing mechanical function of the zygomatic region in macaques: validation and sensitivity testing of finite element models. *Journal of Anatomy* 210: 41–53.
- Lieberman D.E., Polk J.D., Demes B., 2004. Predicting Long Bone Loading From Cross-Sectional Geometry. *American Journal of Physical Anthropology* 123: 156–171.
- Liu J., Shi L., Fitton L.C., Phillips R., O’Higgins P., Fagan M.J., 2011. The application of muscle wrapping to voxel-based finite element models of skeletal structures. *Biomechanics and Modeling in Mechanobiology* 11: 35–37.
- Milne N., Toledo N., Vizcaíno S.F., 2011. Allometric and group differences in the xenarthran femur. *Journal of Mammalian Evolution* 19(3): 199–208. doi:10.1007/s10914-011-9171-0
- Milne N., O’Higgins P., 2012. Scaling of form and function in the xenarthran femur: a 100 fold increase in body mass is mitigated by repositioning of the third trochanter. *Proc. R. Soc. B* 279(1742): 3449–3456. doi:10.1098/rspb.2012.0593
- Moazen M., Curtis N., Evans S.E., O’Higgins P., Fagan M.J., 2009. Biomechanical assessment of evolutionary changes in the lepidosaurian skull. *Proceedings of the National Academy of Sciences, USA* 20: 8273–8277.
- O’Higgins P., Jones N., Ghattaura A., Hammond P., Hutton T., Carr M., 2002. Geometric morphometric approaches to the study of soft tissue growth and expression in the human face. *American Journal of Physical Anthropology Supplement* 34: 119.
- O’Higgins P., Cobb S.N., Fitton L.C., Gröning F., Phillips R., Liu J., Fagan M.J., 2011. Combining geometric morphometrics and functional simulation: an emerging toolkit for virtual functional analyses. *Journal of Anatomy* 218: 3–15.
- O’Higgins P., Fitton L., Phillips R., Shi J.F., Liu J., Groening F., Cobb S.N., Fagan M.J., 2012. Virtual functional morphology: novel approaches to the study of craniofacial form and function. *Evolutionary Biology* 39(4): 521–535. doi:10.1007/s11692-012-9173-8
- Oxnard C.E., O’Higgins P., 2009. Biology Clearly Needs Morphometrics. Does Morphometrics Need Biology? *Biological Theory* 4(1): 1–14.
- Panagiotopoulou O., Wilshin S.D., Rayfield E.J., Shefelbine S.J., Hutchinson J.R., 2012. What makes an accurate and reliable subject-specific finite element model? A case study of an elephant femur. *J. R. Soc. Interface* 9(67): 351–361. doi:10.1098/rsif.2011.0323
- Parr W.C.H., Wroe S., Chamoli U., Richards H.S., McCurry M.R., Clausen P.D., McHenry C., 2012. Toward integration of geometric morphometrics and computational biomech-

- anics: New methods for 3D virtual reconstruction and quantitative analysis of Finite Element Models. *Journal of Theoretical Biology* 301: 1–14.
- Pauwels. 1980. *Biomechanics of the locomotor apparatus: Contributions on the functional anatomy of the locomotor apparatus*. Springer-Verlag, Berlin.
- Pierce S.E., Angielczyk K.D., Rayfield E.J., 2008. Patterns of morphospace occupation and mechanical performance in extant crocodylian skulls: a combined geometric morphometric and finite element modeling approach. *Journal of Morphology* 269: 840–865.
- Rayfield E.J., 2005. Using finite-element analysis to investigate suture morphology: a case study using large carnivorous dinosaurs. *Anatomical Record* A283: 349–365.
- Rybicki E.F., Simonen F.A., Weis E.B., 1972. On the mathematical analysis of stress in the femur. *Journal of Biomechanics* 5: 203–215.
- Sigal I.A., Hardisty M.R., Whyne C.M., 2008. Mesh-morphing algorithms for specimen-specific finite element modelling. *Journal of Biomechanics* 41: 1381–1389.
- Sigal I.A., Yang H., Roberts M.D., Downs J.C., 2010. Morphing methods to parameterize specimen-specific finite element model geometries. *Journal of Biomechanics* 43: 254–262.
- Slice D.E., 1999. Geometric motion analysis. *American Journal of Physical Anthropology Supplement* 28: 253–254.
- Slice D.E., 2003. The analysis of shape sequences. *American Journal of Physical Anthropology Supplement* 36: 194–195.
- Stayton C.T., 2009. Application of Thin-Plate Spline Transformations to Finite Element Models, or, How to Turn a Bog Turtle into a Spotted Turtle to Analyze Both. *Evolution* 63: 1348–1355.
- Strait D.S., Richmond B.G., Spencer M.A., Ross C.F., Dechow P.C., Wood B.A., 2007. Masticatory biomechanics and its relevance to early hominid phylogeny: An examination of palatal thickness using finite-element analysis. *Journal of Human Evolution* 52: 585–599.
- Strait D.S., Weber G.W., Neubauer S., Chalk J., Richmond B.G., Lucas P.W., Spencer M.A., Schrein C., Dechow P.C., Ross C.F., Grosse I.R., Wright B.W., Constantino P., Wood B.A., Lawn B., Hylander W.L., Wang Q., Byron C.D., Slice D.E., Smith A.L., 2009. The feeding biomechanics and dietary ecology of *Australopithecus africanus*. *Proceedings of the National Academy of Sciences USA* 106: 2124–2129.
- Taylor M.E., Tanner K.E., Freeman M.A.R., Yettram A.L., 1996. Stress and strain distribution within the intact femur: compression or bending? *Medical Engineering and Physics* 18: 122–131.
- Vollmer D., Meyer U., Joos U., Vegh A., Piffko J., 2000. Experimental and finite element study of a human mandible. *Journal of Cranio-Maxillofacial Surgery* 28: 91–96.
- Weber G.W., Bookstein F.L., Strait D.S., 2011. Virtual anthropology meets biomechanics. *Journal of Biomechanics* 44: 1429–1432.
- Wroe S., Moreno K., Clausen P., McHenry C., Curnoe D., 2007. High-Resolution Three-Dimensional Computer Simulation of Hominid Cranial Mechanics. *The Anatomical Record* 290A: 1248–1255.

Associate Editor: A. Cardini